Experimental and numerical analysis of a helically-coiled solar water collector at various angular placements

Halil İbrahim Variyenli[1], Ali Amini[2], Azim Doğuş Tuncer[3], Ataollah Khanlari[4*], Şahin Kolay[5]

[1]Department of Energy Systems Engineering, Gazi University, Ankara, Turkey

[2]Department of Automotive Engineering, Atılım University, Ankara, Turkey

[3]Energy Systems Engineering, Burdur Mehmet Akif Ersoy University, Burdur, Turkey

[4]Department of Mechanical Engineering, Faculty of Engineering, Tarsus University, Tarsus, Mersin, Turkey

[5]Natural and Applied Science Institute, Gazi University, Ankara, Turkey

*Corresponding author: Ataollah Khanlari (ata_khanlari@yahoo.com)

Abstract

Solar water collectors are widely utilized for providing hot water to be used in different applications. In this work, a solar water collector with a helically coiled absorber has been designed, fabricated, and examined at different test conditions to specify its overall performance. One of the major goals of using a tube-type absorber is to upgrade the thermal efficiency of the collector by providing a perpendicular angle between the absorber and incident solar rays. Also, using a helically-coiled structure make it possible to increase the absorber surface in a relatively small volume in comparison to conventional solar water collectors. In the first step of this research, the designed helically-coiled solar collector has been simulated using a solar radiation model. In the next step, the manufactured helically-coiled solar collector has been experimentally tested at three different inclination angles and various water flow rates. According to the experimental results, mean thermal efficiencies of horizontal, vertical, and angular

helically-coiled collectors were obtained in the ranges of 29.48-48.23%, 27.17-47.03%, and 32.50-52.71%, respectively. In addition, sustainability index values for horizontal, vertical and angular helically-coiled collectors were achieved between the ranges of 1.0041-1.0091, 1.0039-1.0087, and 1.0043-1.0102, respectively. Moreover, the maximum deviation between numerical and experimental findings was calculated as 14%.

Keywords: Solar water collector; helically-coiled; angular placement; solar radiation model.

Nomenclature	
A	Area (m^2)
C_p	Specific heat capacity of water (kJ/kg.K)
D_h	Hydraulic diameter (m)
$\dot{Ex}$	Exergy rate (W)
h	Heat transfer coefficient ($W/m^2.K$)
I	Solar radiation (W/m^2)
k_w	Thermal conductivity (W/m.K)
$\dot{m}$	Mass flow rate (kg/s)
Nu	Nusselt number (-)
$\dot{Q}$	Useful thermal energy (W)
Re	Reynolds number (-)
T	Temperature (°C)
SI	Sustainability index (-)
u_i	Velocity (m/s)
w_1, w_2, w_n	Uncertainties in the independent variables
W_R	Total uncertainty (%)
Greek letters	
μ_w	Dynamic viscosity (Pa.s)
ρ_w	Density of water (kg/m^3)

η_e	Exergy efficiency (%)
η_t	Thermal efficiency (%)
Subscripts	
a	ambient
i	inlet
o	outlet
s	sun
w	water

1. Introduction

Nowadays, a big part of global energy demand is supplied using fossil resources, and growing industries caused a huge increase in energy demand in the world. Also, fossil fuel resources are limited and alternative energy sources should be found for the future. In addition, the utilization of fossil fuels has significant negative environmental effects that should be taken into the consideration (Selimefendigil et al., 2022). Renewable energy sources could be good alternatives to fossil fuels because they are sustainable and clean energies. Also, solar energy is known as a primary energy source and could be utilized to supply a big part of the needed energy in the world. Incoming solar rays could be converted to useful energy using photovoltaic panels or thermal systems such as solar air and water collectors (Gorjian et al., 2021; Selimefendigil and Şirin, 2022; Akbar et al., 2021).

Solar air and water collectors are widely utilized in different applications to provide hot air and hot water due to their high thermal efficiency and low cost. In the last years, different types of solar water collectors like evacuated tube and flat plate collectors are extensively utilized to supply hot water. In a study, Pathak et al. (2019a) developed a dual-purpose

solar collector in order to the simultaneous production of hot water and hot air. Different techniques have been applied in order to upgrade the thermal performance of various types of solar collectors (Ghodbane et al., 2021; Sheikholeslami et al., 2021b). Also, some researchers utilized phase change materials to increase the utilization time period of solar energy-based systems (Li, 2015 and 2016; Li and Zheng, 2016). In addition, nanofluids can be used as working fluid in solar collectors in order to upgrade thermal efficiency (Xiong et al., 2021a; Aytaç, 2022a, 2022b). Ramanathan (2020) proposed a new vortex producer for heat transfer improvement in a sudden expansion channel utilized as a solar water collector. Sheikholeslami and Jafaryar (2023) utilized helical-type turbulators and nanoparticles in order to improve the overall performance of a concentrated solar collector. Zou et al. (2023) numerically investigated the potential of using nanoparticles on the energy harvest increment in a solar collector. Rani and Tripathy (2022) designed and integrated semicircular loop fins in order to increase the efficiency of a solar collector. Kansara et al. (2021) investigated the effects of using porous media and internal fins on the efficiency increasing of a flat plate-type collector utilizing experimental and numerical methods. Sheikholeslami and Ebrahimpour (2022) utilized Al_2O_3-water nanofluid as a working fluid in a linear Fresnel solar collector for improving thermal performance. Almeshaal et al. (2020) utilized twisted tape turbulators in order to improve the thermal performance of a solar water collector. Gholipour et al. (2020) designed and manufactured new absorbent tubes arrangement for improving the performance of vacuum tube collectors. In another work, Gholipour et al. (2021) utilized new types of vacuum U-tube type collectors and improved their efficiency by utilizing nanofluid. In the last years, different types of tubular solar collectors have been developed to be used in

various applications (El-Said et al., 2022; Hassan et al., 2020; Abo-Elfadl et al., 2020). In addition, some researchers stated that applying a tube-type absorber could upgrade the thermal effectiveness of the collector by providing a perpendicular angle between the absorber and incident solar rays (Afshari et al., 2020; Sözen et al., 2020; Abo-Elfadl et al., 2021).

Different from conventional solar water collectors, Goudarzi et al. (2014) manufactured a helically coiled solar collector and tested it with water and CuO-water nanofluid. In another study, Goudarzi et al. (2015) experimentally examined the performance of a horizontally oriented helically coiled solar collector using two different nanofluids. Shojaeizadeh et al. (2021) developed a helically coiled solar water heater and improved its efficiency using nanofluid under a magnetic field. Chakraborty et al. (2021) numerically designed a helical absorber tube for a parabolic solar trough collector to increase thermal efficiency. Swanepoel et al. (2021) designed a new helically coiled receiver for direct steam generation in a concentrated type collector. Raut et al. (2022) examined the potential of solar energy storage by using a helically coiled tube placed inside a shell filled with paraffin material.

Some researchers applied different numerical methods to specify the thermal and flow behavior of various types of energy systems like solar collectors and drying systems (Malan et al., 2003; Lewis and Malan, 2005; Çiftçi et al., 2021; Eker et al., 2021). In some studies fin modification was proposed in order to increase the thermal performance (Yıldırım et al., 2021). Singla et al. (2022) used the CFD approach to examine the flow and thermal characteristics of a rib roughened evacuated pipe-type solar heater for hot air production. Sheikholeslami and Farshad (2021) numerically analyzed the heat transfer

enhancement potential of a solar collector including different turbulators using hybrid-type nanofluids. In another numerical work, Sheikholeslami et al. (2021a) used the Ansys Fluent software to model the thermal characteristics of nanofluid in a solar water collector at turbulent flow regime. Saedodin et al. (2021) numerically surveyed the impact of adding different types of turbulators over the tube of a parabolic trough collector on the total effectiveness of the system. Awasthi and Khan (2019) used the Ansys Fluent software to simulate the overall performance of a coiled tube-type absorber of a concentrating solar collector. Xiong et al. (2021b) numerically modeled the thermal behavior of a flat plate type collector with hybrid-type nanofluids as working fluid.

Investigating available studies in the literature shows the potential of tube-type absorbers in different solar collectors. Also, helically coiled absorbers were used in some applications in order to improve absorber surface area and consequently upgrade thermal efficiency. In the present work, a solar water collector with a helically coiled absorber has been designed, manufactured, and experimentally examined at different conditions to specify its overall effectiveness. The developed helically coiled solar collector has been tested at three different inclination angles to specify the effect of orientation. The general structure of the present work is given in Fig. 1.

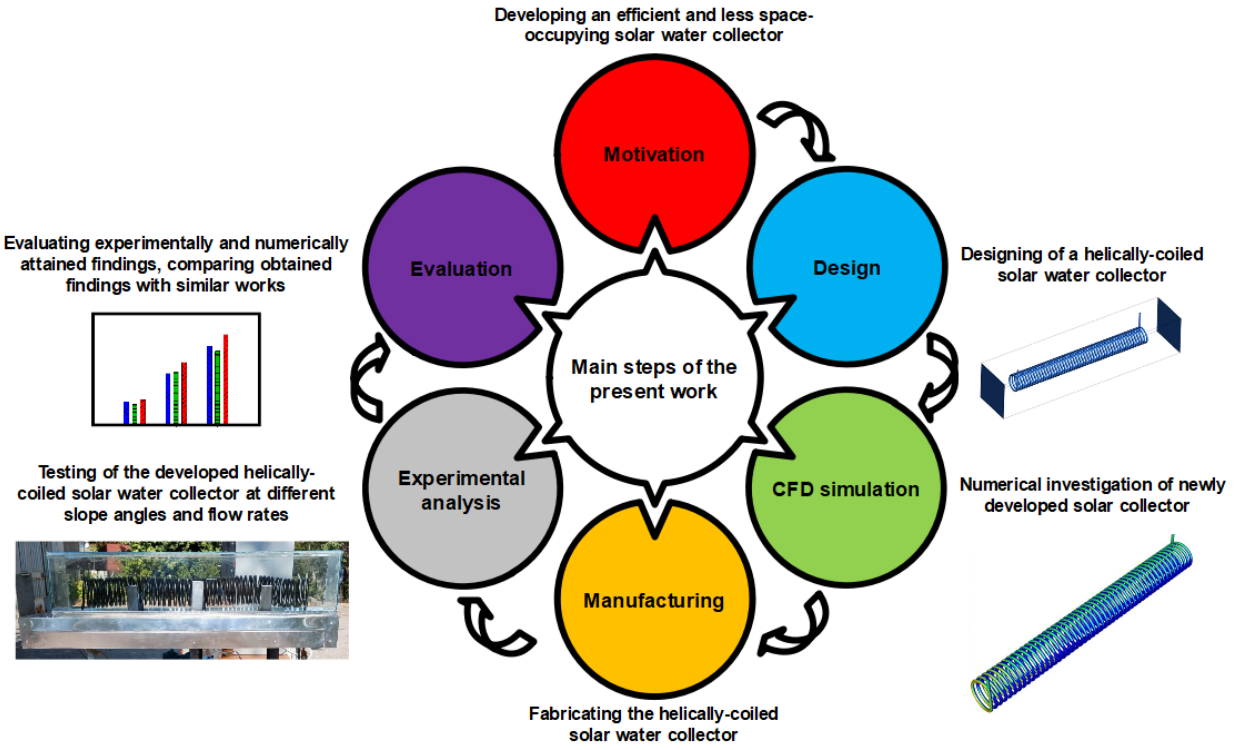

Fig. 1. General structure of the present study

2. Numerical Analysis

2.1. Flow and Heat Analysis

2.1.1. Analyzed geometry

Ansys Workbench software has been utilized to investigate the flow of water inside the spiral tube and solar heat absorption. The CAD geometry has been composed in the Design Modeler module of Ansys Workbench (Fig. 2). In the designed geometry of the solar collector water, copper tube, air chamber and isolation glass wall domains have been created.

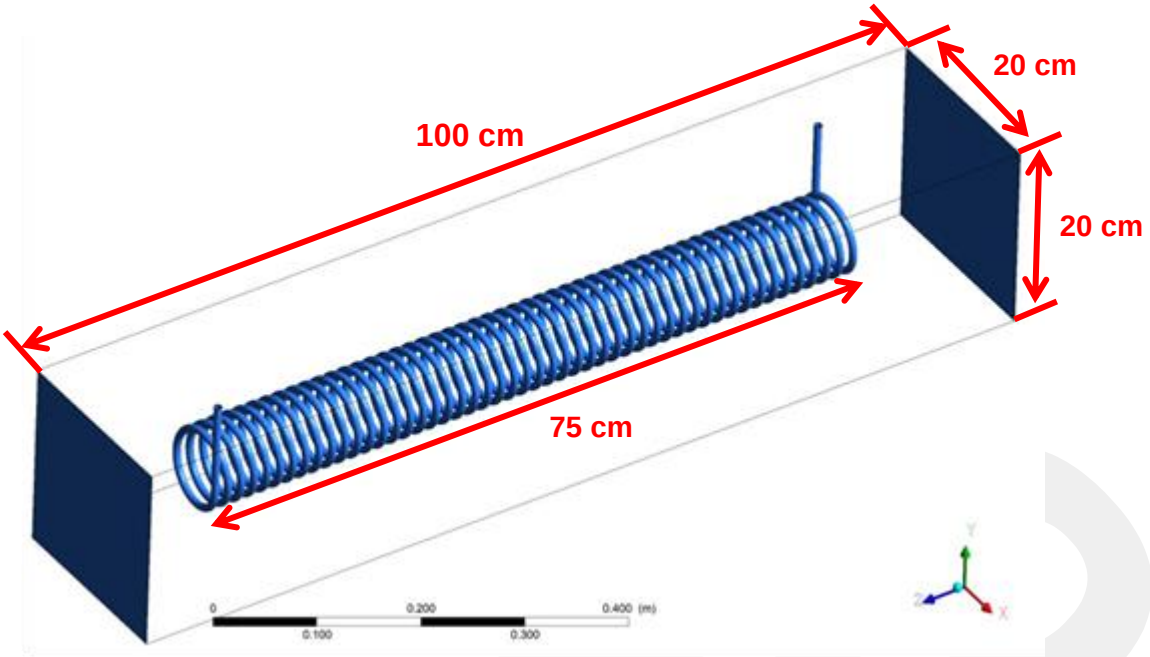

Fig. 2. Collector geometry

2.1.2. Mesh study

The mesh configuration of the defined system was performed in the Mesh module of ANSYS program. In this context, an element size of 0.8 mm has been applied for the water zone with selecting refinement and surface sizing adjacent to the walls and edges (Fig. 3). As the contact zone of air and tube which is critical in absorbing solar energy, the meshing operation of this area was done by a finer element size.

In order to present criteria for mesh quality of the system, the Skewness number of mesh structures has been evaluated. Fig. 4 illustrates the whole domain mesh configuration statistics data. The mean and maximum values of the skewness meter are 0.28 and 0.93 respectively. It should be stated that the maximum acceptable value of the skewness parameter is 0.98 for flow analysis. It could be concluded that the presented mesh of the system has good quality. Whole mesh structure has about 6,195,000 Nodes and

24,586,000 Elements. The numerical simulations have been performed by using a personal computer with a 3.7 GHz processor and 64 GB RAM.

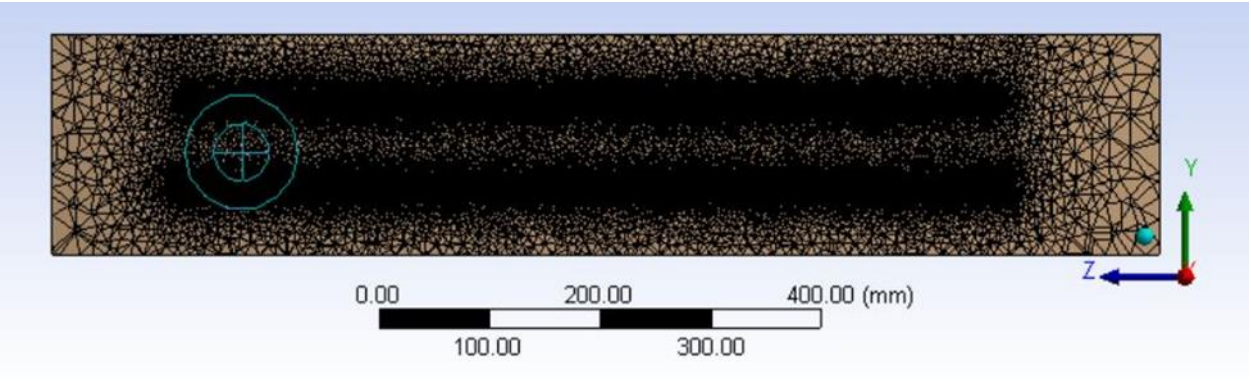

(a)

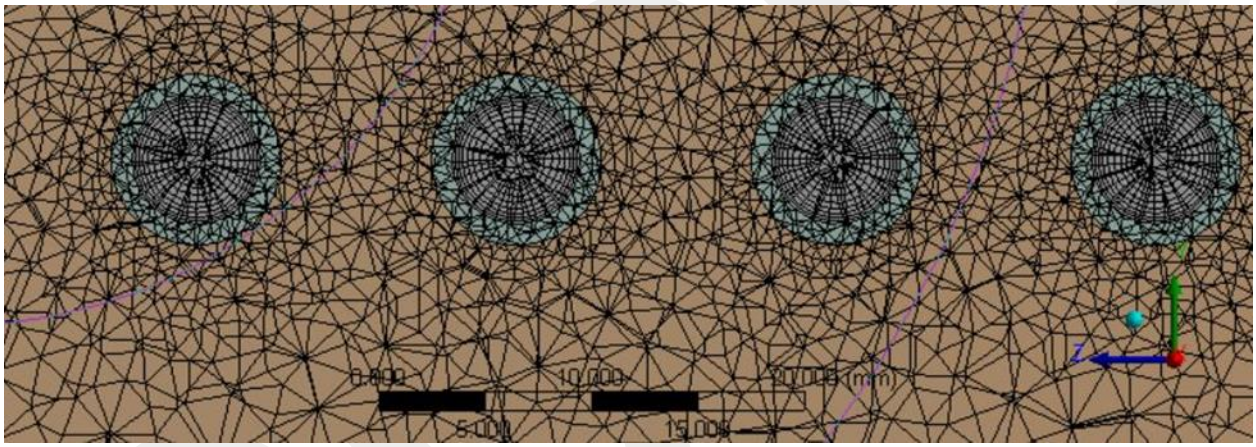

(b)

Fig. 3. The section view of mesh structure (a) all domains (b) water and tube contact

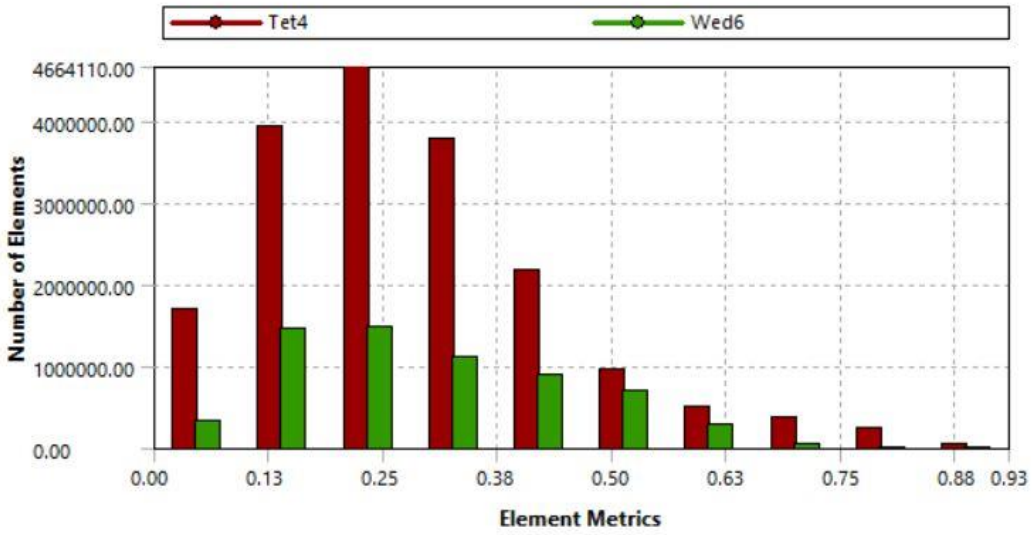

Fig. 4. The whole domain mesh structure statistics data

In order to study the mesh independency of analysis, 4 different cell sizes have been selected for the water domain and flow analysis was performed to calculate the pressure drop inside the spiral tube (Table 1). The volumetric flow rate for this case study was 1.5 lpm. As it can be seen from Table 1 data, mesh finning processes is started from Mesh1 to Mesh4. Approximately 25 % refining in element size is tracked and numerical analyses were done for 4 mesh structures. According to de numerical results, deviation in pressure difference has been reduced by using a finer mesh structure. As the pressure difference deviation between Mesh3 and Mesh4 is 0.9%, therefore Mesh3 structure has been selected as an acceptable mesh configuration for model analysis.

Table 1. Mesh independency study on water domain

	Mesh1	Mesh2	Mesh3	Mesh4
Element size	5,900,000	7,100,000	8,550,000	10,785,000
Element difference (%)	-	25	25	26.1
Pressure drop (kPa)	45	55	58.67	59.20
Pressure difference (%)	-	22.2	6.6	0.9

2.1.3. Boundary Conditions

Boundary conditions of the domain consist of water inlet mass, convection heat loss, and solar radiation. In the numerical analysis of helically-coiled solar collectors, 3 different water volume flows were studied (1.5, 1, and 0.5 lpm). Solar irradiation with a defined sun direction vector has been employed on transparent glass walls. All six sides of the collector have been covered by 4 mm thickness glass walls with 0.1 absorptivity and 0.8 transmissivities which are defined as solar boundary conditions. The surrounding of the collector has been defined by the environment with 20°C temperature and convective heat transfer coefficient of 5 $W/m^2.K$. According to the experimental study of Amini et al. (2021), the natural cooling process of a hot object (heat loss to surrounding) in standard environmental conditions without forced convection effect can be modeled by a convection coefficient of 3-7 $W/m^2.K$. Therefore this study is using average convective heat transfer coefficient of 5 $W/m^2.K$. Solar irradiation values were taken between 650-900 W/m^2 because the experiments were conducted at different days. In addition, the radiation heat loss of the collector to the surrounding has been modeled by semi-transparent walls with a 0.1 emissivity coefficient.

2.1.4. Analysis

Flow and thermal analysis of the helically-coiled collector has been performed in the Fluent module of ANSYS software. Accordingly, steady-state, pressure-based flow with the $k-\varepsilon$ turbulent model has been utilized. Also, standard air and water liquid were selected as working fluids. In order to apply sun irradiation on the collector, the radiation model toolbox of Fluent has been used by activating the surface-to-surface model. This model is widely utilized in different researches (Sarper et al., 2018a; 2018b). Sun direction vector has been defined according to the angular position of the device. According to the initial results, the maximum temperature difference between the inlet and outlet sections of the water line was recorded at about 2 degrees. Therefore, the dependency of fluid properties on temperature has not any significance in this case. In addition, to achieve accurate numerical findings, the convergence absolute criteria for continuity, x-velocity, y-velocity, and z-velocity were defined as 1e-3. Also, the convergence criteria for energy equation residuals was defined as 1e-7.

Continuity and momentum equations are solved in the fluid domain to calculate the velocity (u, v, and w) and pressure (P) values in each cell. The continuity equation for the case of constant density (ρ) conditions can be expressed as follows (Cengel and Cimbala, 2013):

$$\frac{\partial u}{\partial x}+\frac{\partial v}{\partial y}+\frac{\partial w}{\partial z}=0 \quad (1)$$

The momentum equations on the three-axis (x, y and z) have been solved simultaneously. As an example, the x momentum equation can be presented as the following form:

$$\rho\left(u\frac{\partial u}{\partial x}+v\frac{\partial u}{\partial y}+w\frac{\partial u}{\partial z}\right)=\rho g_x-\frac{\partial P}{\partial x}+\frac{\partial}{\partial x}\left(2\mu\frac{\partial u}{\partial x}+\lambda\vec{\nabla}.\vec{V}\right)+\frac{\partial}{\partial y}\left[\mu\left(\frac{\partial u}{\partial y}+\frac{\partial v}{\partial x}\right)\right]+\frac{\partial}{\partial z}\left[\mu(\frac{\partial w}{\partial x}+\frac{\partial u}{\partial z})\right] \quad (2)$$

The standard $k-\varepsilon$ turbulence model (SKE) is the most widely-utilized turbulence model for different engineering applications (Nithiarasu et al., 2016; Afshari et al., 2021; Khanlari et al., 2022). It should be stated that $k-\varepsilon$ turbulence model is extensively utilized in the modeling of similar solar collectors and its accuracy was addressed in various pieces of research (Sheikholeslami and Ebrahimpour, 2022; Sheikholeslami et al., 2022). Utilizing data from numerous benchmark trials, such as pipe flow, model parameters are calibrated. It is a powerful and accurate model for a wide range of engineering applications. The transport equation for turbulence energy k can be given as (Ansys, 2017):

$$\frac{\partial(\rho k)}{\partial t}+\frac{\partial(\rho\bar{u}_i k)}{\partial X_i}=-\rho\overline{\acute{u}_\iota\acute{u}_J}\frac{\partial\bar{u}_i}{\partial t}-\rho\varepsilon+\frac{\partial}{\partial X_i}\left[(\mu+\frac{\mu_t}{\sigma_k})\frac{\partial k}{\partial X_i}\right] \quad (3)$$

This requires a dissipation rate, ε, which is completely modeled phenomenologically (not derived) and could be expressed as:

$$\frac{\partial(\rho\varepsilon)}{\partial t}+\frac{\partial(\rho\bar{u}_i\varepsilon)}{\partial X_i}=C_{1\varepsilon}P_k\frac{\varepsilon}{k}-C_{2\varepsilon}\rho\frac{\varepsilon^2}{k}+\frac{\partial}{\partial X_j}\left[(\mu+\frac{\mu_t}{\sigma_\varepsilon})\frac{\partial\varepsilon}{\partial X_j}\right] \quad (4)$$

Dimensionally, the dissipation rate (ε) which is related to k and a turbulence length scale (L_t) and could be given as:

$$\varepsilon=\frac{k^{3/2}}{L_t} \quad (5)$$

Together with the k equation, eddy viscosity (μ_t) could be defined as:

$$\mu_t=\rho C_\mu L_t\sqrt{k}=\rho C_\mu\frac{k^2}{\epsilon} \quad (6)$$

The energy equation is solved in the fluid domain to obtain the temperature (T) distribution in the domain.

$$\rho c_p\left(u\frac{\partial T}{\partial x}+v\frac{\partial T}{\partial y}+w\frac{\partial T}{\partial z}\right)=\vec{\nabla}.k\,\vec{V}\,T+\varphi \quad (7)$$

φ is the energy source or sink function and c_p denotes the specific heat capacity of materials in the solution domain. Spiral tube surfaces and glass wall surfaces can absorb part of solar irradiation. The radiation analysis of the domain, either the temperature of each surface is calculated according to the following equations (Çengel and Ghajar, 2020):

$$\dot{Q}_\iota = A_i \sum_{j=1}^{N} F_{i\to j}(J_i - J_j) \quad (8)$$

$$\sigma T_i^4 = J_i + \frac{1-\epsilon_i}{\epsilon_i} \sum_{j=1}^{N} F_{i\to j}(J_i - J_j) \quad (9)$$

The view factor of $F_{i\to j}$ shows the percentage of radiation that is leaving surface i that strikes surface j. The radiosity is the total radiation energy that leaves a surface per unit of time and per unit of area, and it is represented by the J value. N is the number of surfaces in the domain.

3. Material and Method

3.1. Experimental Apparatus

In this research, a newly developed helically-coiled solar collector has been developed, manufactured, and analyzed. In this regard, the copper tube has been utilized to develop a helically-coiled tube to be used in the solar collector. The utilized copper tube has a diameter of 8 mm. Also, the developed helical coil has a diameter of 85 mm. Moreover, coil pitch and the total number of coil turn values are 15 mm and 49, respectively. One of the main goals of using a tube-type absorber is to upgrade the thermal efficiency of the collector by providing a perpendicular angle between the absorber surface and incident solar rays. In other words, tubular absorber surfaces are always perpendicular to the sun's rays for most of the day. Also, using a helically-coiled structure make it possible to

247 increase the absorber surface in a relatively small volume in comparison to conventional
248 (flat plate type) solar water collectors. The structured helical coil was painted with an
249 industrial matt black paint with 95% absorptivity. A glass rectangular prism has been
250 utilized as a casing material for the collector with a thickness of 4 mm and a transmissivity
251 of 92%. A reflector plate has been utilized on the bottom of the casing in order to reflect
252 sun rays to the bottom side of the helically-coiled absorber tube. Moreover, the bottom
253 side of the developed collector has been thermally insulated in order to prevent heat
254 losses from the back of the collector. Fig. 5 represents a schematic view of the
255 experimental apparatus and a view of investigated inclination angles. In addition, Fig. 6
256 illustrates a photograph of the utilized experimental setup.

GCRIS

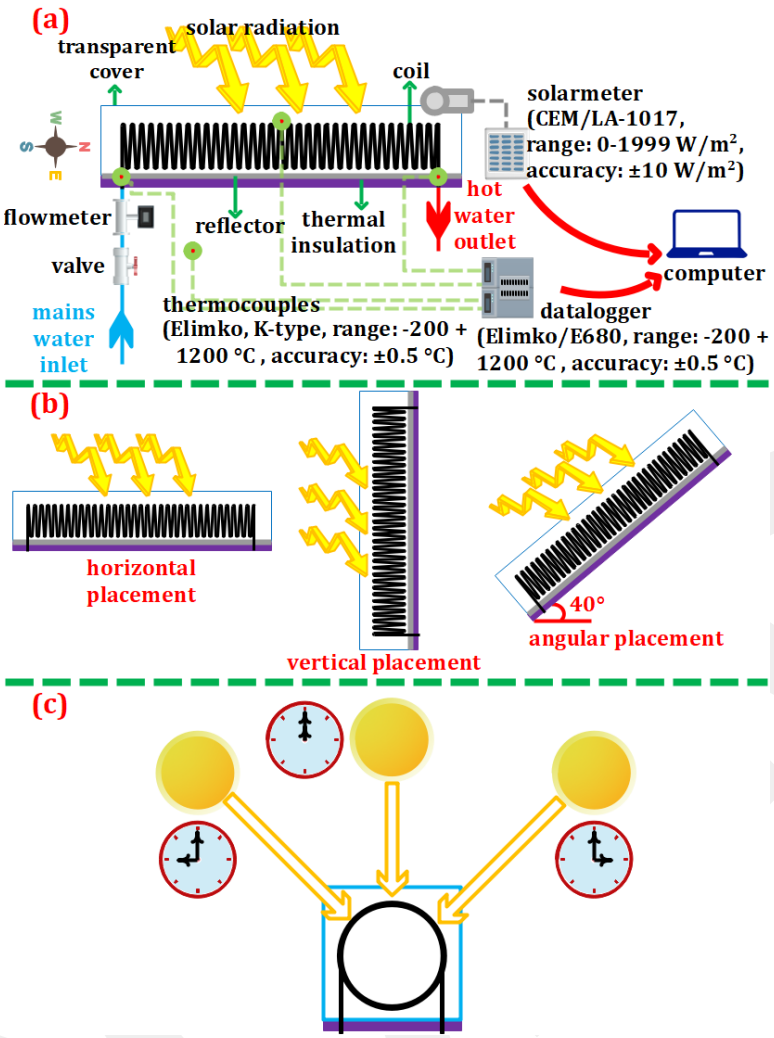

257

258 **Fig. 5.** (a) Schematic view of the experimental setup, (b) view of investigated inclination

259 angles, c) incoming sun rays over the collector during the tests



Fig. 6. A photograph of the experimental apparatus

3.2. Experimental Procedure

The designed and manufactured helically-coiled solar water collector has been tested in Ankara, Turkey in September and October 2021. As stated above, the effects of inclination angle and water flow rate have been investigated in this work. Accordingly, the developed helically-coiled solar water collector has been tested at three different inclination angles to specify the effect of slope angle on the energetic and exergetic performances. Exps. 1-3, Exps. 4-6, and Exps. 7-9 have been done at the horizontal, vertical, and angular orientation of the solar water collector, respectively. In the angular orientation of the solar water collector, a 40° tilt angle has been selected which corresponds to the yearly tilt angle of the test region. Each orientation has been experimentally tested at three different volumetric water flow rates including 1.5, 1.0, and 0.5 lpm which approximately correspond to 0.025, 0.0167, and 0.0084 kg/s mass flow rates. In other words, the performance tests have been conducted at 9 days.

Corresponding Reynolds numbers in the experiments done at 1.5, 1.0, and 0.5 lpm are 5300, 3530, and 1760. Moreover, Dean number varied between 465-1410 in the experiments. Helically coiled collector's inlet fed by mains water. A helically coiled water collector has been covered with fabric and oriented to the south before starting the performance experiments. In other words, before starting the experiments, the solar-receiving surface of the collector was covered with fabric and water started to circulate inside the system. Then, the inlet water's volumetric flow rate has been adjusted using a flowmeter, and water was entered into the collector. Water has been circulated in the covered collector for 15 minutes before starting the tests. This process has been done with the aim of obtaining a steady regime in the tested solar collector. This technique is aimed to obtain a steady fluid flow inside the collector. In addition, this process makes it possible to obtain accurate results. In other words, covering the solar-receiving surface of the collector prevent harvesting energy by the system before starting the experiments. The fabric cover of the solar water collector has been removed and the performance tests have been started at 10:00 and ended at 16:00. Temperature values have been recorded at the collector inlet, collector outlet, helically coiled surface, and the surrounding air. Accordingly, temperature measurements have been recorded every 5 seconds. Also, solar radiation values have been measured every 15 minutes from the top surface of the collector. Measurement points can be seen in Fig. 5.

3.3. Theoretical calculations

In the present research, the designed and manufactured helically coiled water collector has been investigated using energy and exergy analyses. As known, dimensionless

numbers have been frequently utilized in analyzing thermal systems. Dimensionless Reynolds and Nusselt numbers can be obtained using Eqs. (10)-(11) (Fattahi and Karimi, 2022):

$$Re = \frac{\rho_w u_i D_h}{\mu_w} \quad (10)$$

$$Nu = \frac{hD_h}{k_w} \quad (11)$$

Also, Dean number is another dimensionless number which is utilized in investigating flow in helically coiled tube and can be found as:

$$De = Re\left(\frac{d_{in}}{D_{coil}}\right)^{0.5} \quad (12)$$

In Eq. (12), d_{in} denotes the inner diameter of the helically coiled tube.

Useful energy gained by the water collector could be achieved as:

$$\dot{Q} = \dot{m}C_p\left(T_{w,o} - T_{w,i}\right) \quad (13)$$

The thermal efficiency of the solar water collector is an important parameter in evaluating the overall performance and can be achieved as:

$$\eta_t = \frac{\dot{Q}}{IA} \quad (14)$$

Exergy expression is a combination of the first and second laws of thermodynamics. Exergy analysis is generally used in designing steps of thermal systems. The general expression of exergy could be given as follows (Wong, 2000; Kotas, 1995):

$$\sum \dot{E}x_{i,net} - \sum \dot{E}x_{o,net} = \sum \dot{E}x_{loss} \quad (15)$$

Exergy efficiency can be obtained utilizing the following equation (Yazdanpanahi et al., 2015):

$$\eta_e = \frac{\sum \dot{E}x_{o,net}}{\sum \dot{E}x_{i,net}} = 1 - \frac{\sum \dot{E}x_{loss}}{\sum \dot{E}x_{i,net}} \quad (16)$$

The net inlet exergy of the solar water collector could be obtained using Eq. (17) (Petela, 2003):

$$\sum \dot{E}x_{i,net} = IA\left[1 - \frac{4}{3}\left(\frac{T_a}{T_s}\right) + \frac{1}{3}\left(\frac{T_a}{T_s}\right)^4\right] \quad (17)$$

Also, the net outlet exergy of the solar water collector can be calculated as (Yazdanpanahi et al., 2015; Tiwari et al. 2009):

$$\sum \dot{E}x_{o,net} = \dot{Q}\left(1 - \frac{T_a}{T_{w,o}}\right) \quad (18)$$

The sustainability index is another exergy-based factor that could be calculated using Eq. (19) (Caliskan, 2017):

$$SI = \frac{1}{1-\eta_e} \quad (19)$$

Experimental uncertainty is also an important indicator in evaluating experimental results and can be obtained (Afshari et al., 2019; Khanlari et al., 2021):

$$W_R = \left[(\frac{\partial R}{\partial x_1}w_1)^2 + (\frac{\partial R}{\partial x_2}w_2)^2 + \cdots + (\frac{\partial R}{\partial x_n}w_n)^2\right]^{1/2} \quad (20)$$

In the present study, calculated average uncertainty values for temperature, solar radiation and thermal efficiency are ±0.64°C, ±17.10 W/m^2 and ±1.82%, respectively.

4. Results and discussion

4.1. Simulation results

Numerical simulations of the developed helically-coiled collector have been performed at different orientation angles and flow rates to present the overall performance of the system at various conditions. Fig. 7 presents the pressure drop in the water domain when the water volumetric flow rate is 1.5 lpm. The outlet pressure of the water tube is zero relative pressure. The highest pressure difference, in the given case, is 58.7 kPa. Fig. 8

presents the velocity distribution in both the water and air domain of the collector. The air domain of the collector has the highest values of velocity because the temperature difference causes a natural convection swirl motion in this zone. The water domain of collector has the average value of 0.88 (m/s) velocity in case of 1.5 (lpm) volumetric flow rate. It should be noted that the air circulation model has not been considered in the collector because the aim of this design is focused on the water stream rather than the air stream. Air zone with glass walls in this model is acting as a medium with low conductivity that minimizes the effect of surrounding air conditions. Also, the thermo-physical properties of air are considered constant values in this simulation. The natural convection or air recirculation effect maybe has some effect on heat flow but it can be neglected besides the important role of radiation on helically coiled that has high absorptivity.

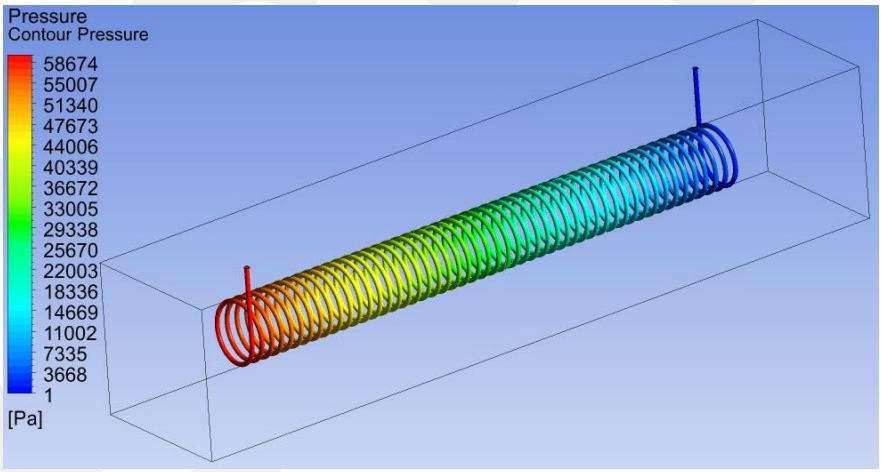

Fig. 7. Pressure contour of water domain (flow rate=1.5 lpm)

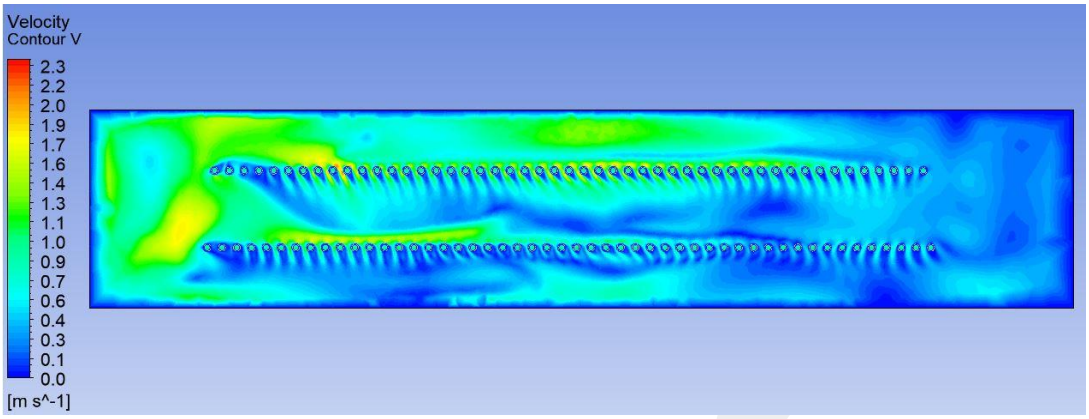

Fig. 8. Velocity contour of air and water domain

In this study, a solar radiation model has been applied in order to simulate a helically-coiled solar collector instead of using constant heat flux which is widely used in the literature. Applying heat flux is an approach to model solar energy-based systems. However, applying the solar radiation model could give similar results to the experimental findings. Fig. 9 represents solar heat flux over the helically-coiled tube of the solar collector at three different orientation angles. The difference between the three orientations of the solar collector is clearly seen in Fig. 9. In other words, this figure represents the effect of the orientation of the helically-coiled solar water collector. Evaluating solar heat flux distribution over the helically-coiled tube illustrates the high potential of angular placement of the collector in gaining solar energy in comparison with other placements.

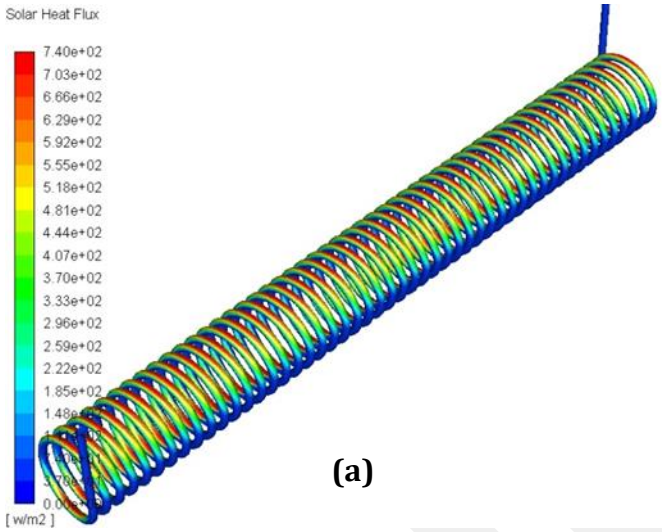
Solar Heat Flux
7.40e+02
7.03e+02
6.66e+02
6.29e+02
5.92e+02
5.55e+02
5.18e+02
4.81e+02
4.44e+02
4.07e+02
3.70e+02
3.33e+02
2.96e+02
2.59e+02
2.22e+02
1.85e+02
[w/m2]

(a)

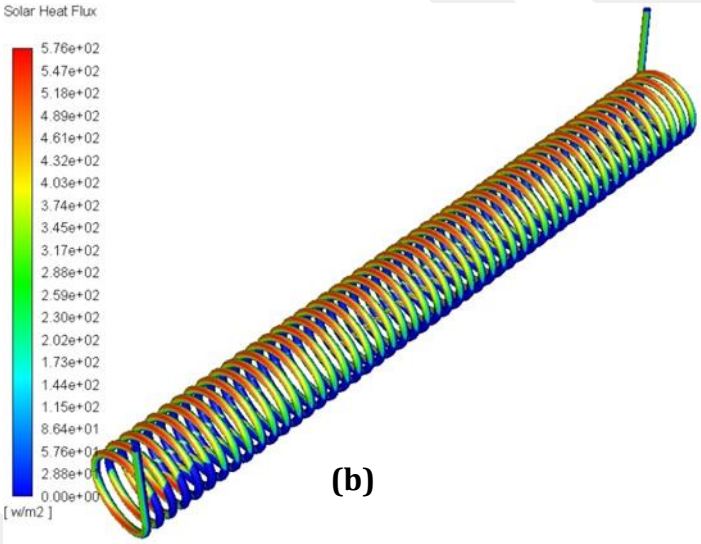
Solar Heat Flux
5.76e+02
5.47e+02
5.18e+02
4.89e+02
4.61e+02
4.32e+02
4.03e+02
3.74e+02
3.45e+02
3.17e+02
2.88e+02
2.59e+02
2.30e+02
2.02e+02
1.73e+02
1.44e+02
1.15e+02
8.64e+01
0.00e+00
[w/m2]

(b)

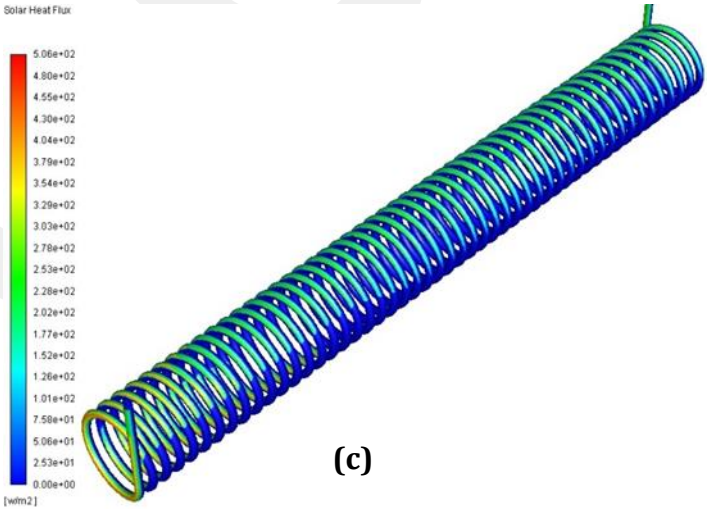
Solar Heat Flux
5.06e+02
4.80e+02
4.55e+02
4.30e+02
4.04e+02
3.79e+02
3.54e+02
3.29e+02
3.03e+02
2.78e+02
2.53e+02
2.28e+02
2.02e+02
1.77e+02
1.52e+02
1.26e+02
1.01e+02
7.58e+01
5.06e+01
2.53e+01
0.00e+00
[w/m2]

(c)

370

Fig. 9. Solar heat flux over the helically-coiled tube of the collector (a) theta=40 (a) theta=0 (a) theta=90

Fig. 10 shows pressure drop values at different water volumetric flow rates and slope angles. Also, the collector has different angular position relative to sun irradiation vector. By increasing the water's volumetric flow rate, the pressure drop in the tube was raised. It means that more pumping power is needed to make the water in circulation.

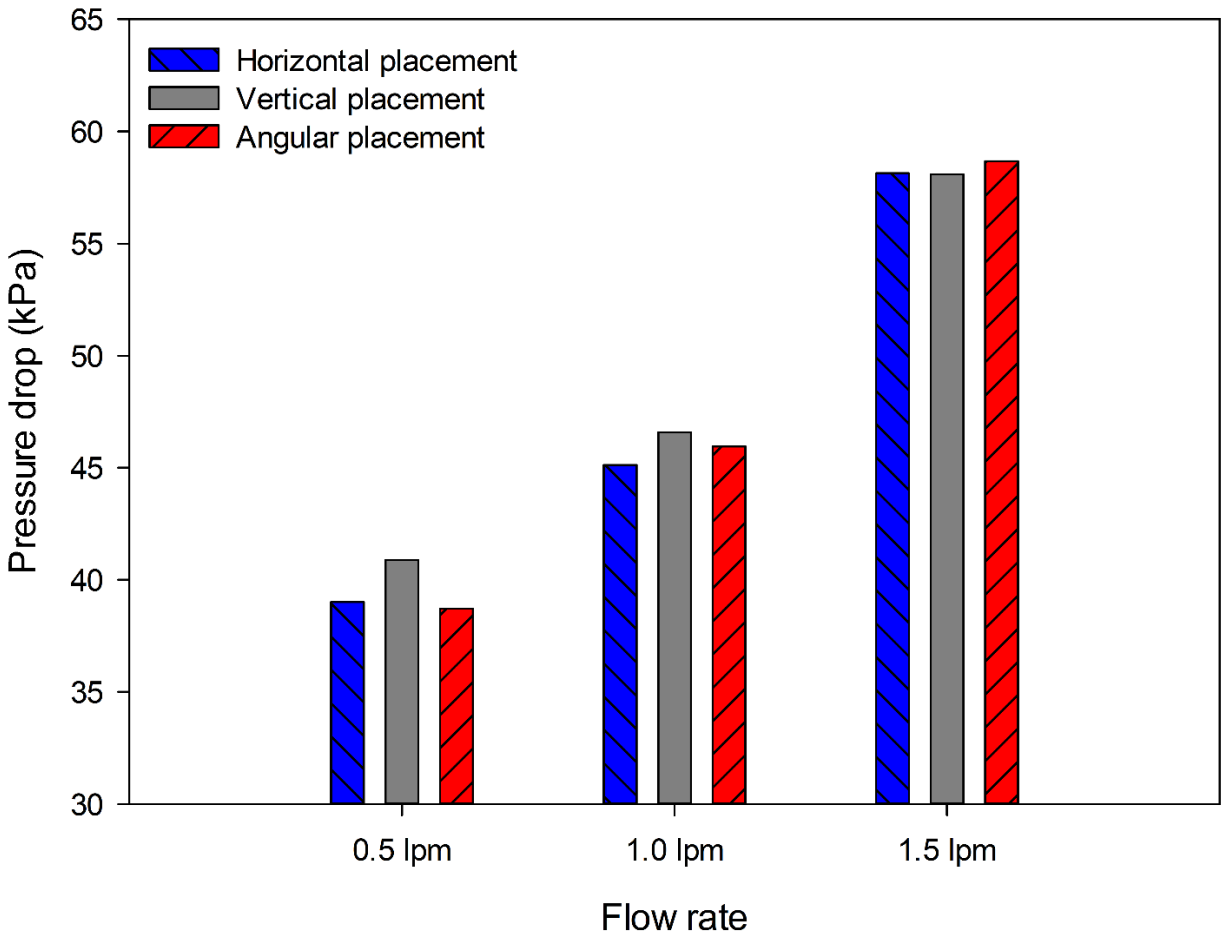

Fig. 10. Numerically obtained pressure drop values

4.2. Experimental results

Experimentally gained results have been provided and thoroughly discussed in this section. As previously noted, an experimental investigation was conducted over a nine-day period at varied flow rates and angular positions. Table 2. represents the experimental case studies according to Dean number. As can be seen in Table 2, the experiments have been conducted at three different flow rates. Also, the geometrical parameters of the solar collector did not vary in the present work. In other words, parameters such as coil diameter and tube diameter were kept constant. Therefore, the only parameter which affects Dean number and Reynolds number is the water mass flow rate.

Table 2. Experimental case studies according to Dean number

Volume flow rate (lpm)	Mass flow rate (kg/s)	Reynolds number	$\frac{d_{in}}{D_{coil}}$	Dean number
0.5	0.0084	1760	0.07	465
1	0.0167	3530	0.07	940
1.5	0.025	5300	0.07	1410

The fluctuation of solar radiation values over local time is shown in Fig. 11. Average solar radiation values in the experiments with the horizontal, vertical, and angular orientation of helically-coiled collector were obtained in the ranges 689-753 W/m^2, 639-656 W/m^2, and 889-899 W/m^2, respectively. Maximum and minimum average solar radiation values were achieved in Exp. 7 and Exp. 6, respectively. Also, the highest instantaneous radiation value was gained as 998 W/m^2 in Exp. 7 at 13:45. It is preferable to state that testing helically-coiled collector at different orientations significantly affected recorded

solar radiation. As stated above, the experiments have been conducted in September and October 2021. The time-dependent fluctuation of environmental temperature values is depicted in Fig. 12. Mean surrounding temperature in Exp. 1, Exp. 2, and Exp. 3 were gained as 24.09°C, 24.44°C and 24.19°C, respectively. Also, mean surrounding temperatures in Exp. 4, Exp. 5, and Exp. 6 were obtained as 22.86°C, 23.60°C, and 22.93°C, respectively. In addition, in the performance tests done with angular orientation of solar collector (Exp. 7, Exp. 8, and Exp. 9) average surrounding temperatures were gained as 24.52 °C, 24.06 °C, and 25.18 °C, respectively. As could be clearly seen, the obtained temperatures are so close to each other.

The inlet water of the collector was provided from the mains water. Therefore, inlet water temperature values showed an alteration during the experiments. Fig. 13 illustrates the time-dependent change of inlet water temperature values.

Inlet water temperature values in the experiments with the horizontal, vertical, and angular orientation of helically-coiled collector were gained in the ranges of 20.76-21.01°C, 20.13-20.87°C, and 19.54-20.55°C, respectively.

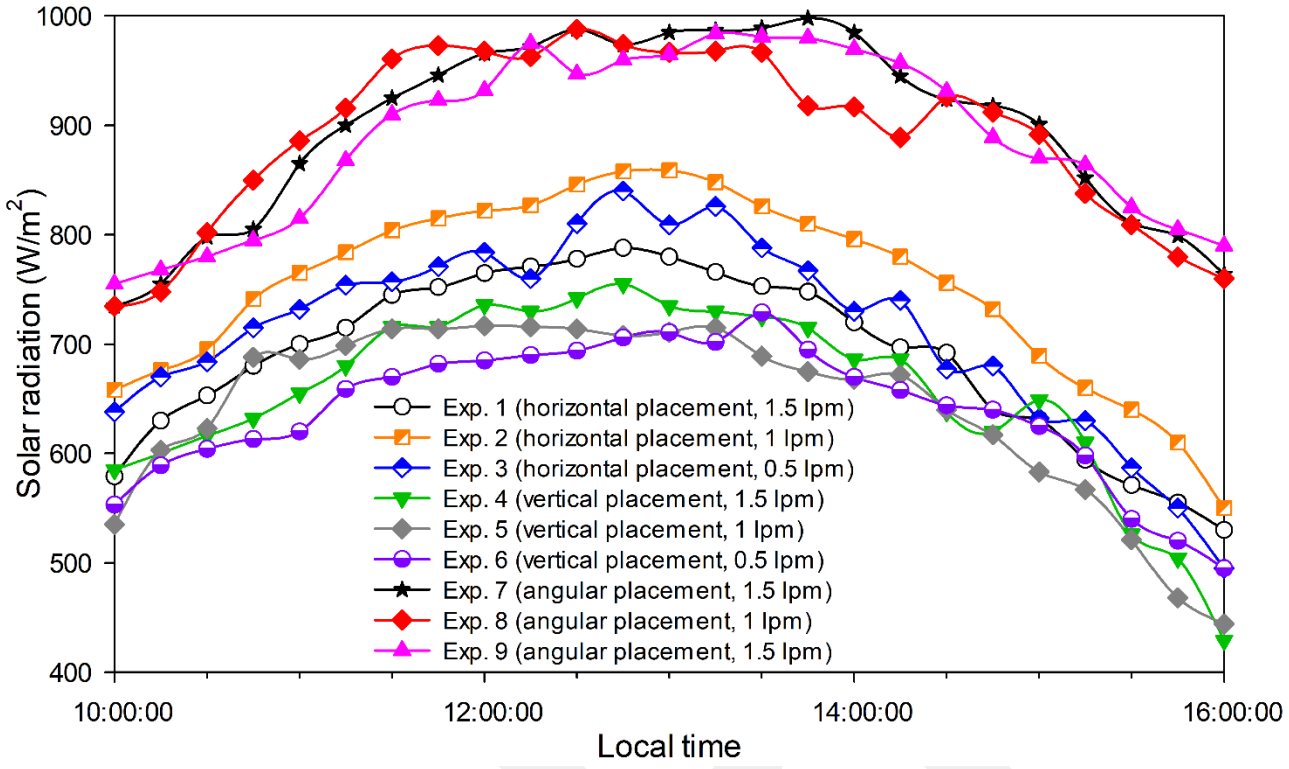

Fig. 11. Time-dependent change in measured daily radiation values

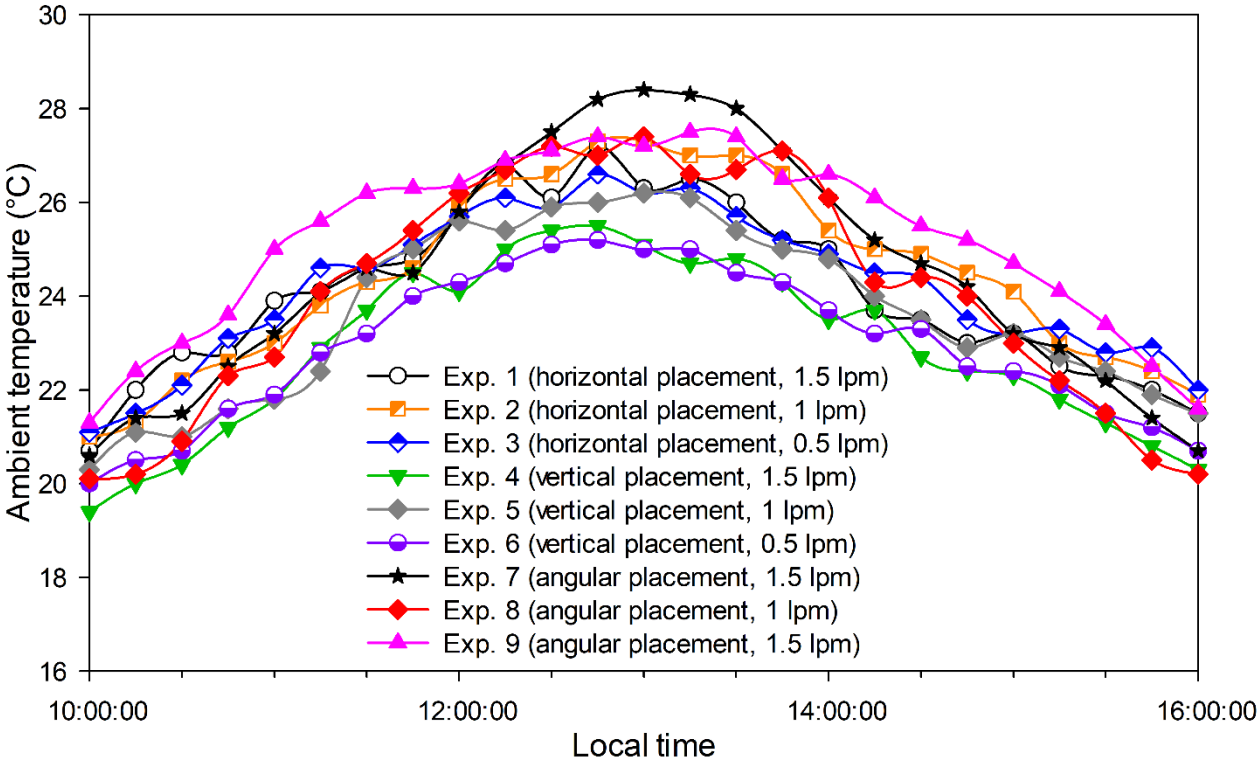

Fig. 12. Time-dependent change in ambient temperature values

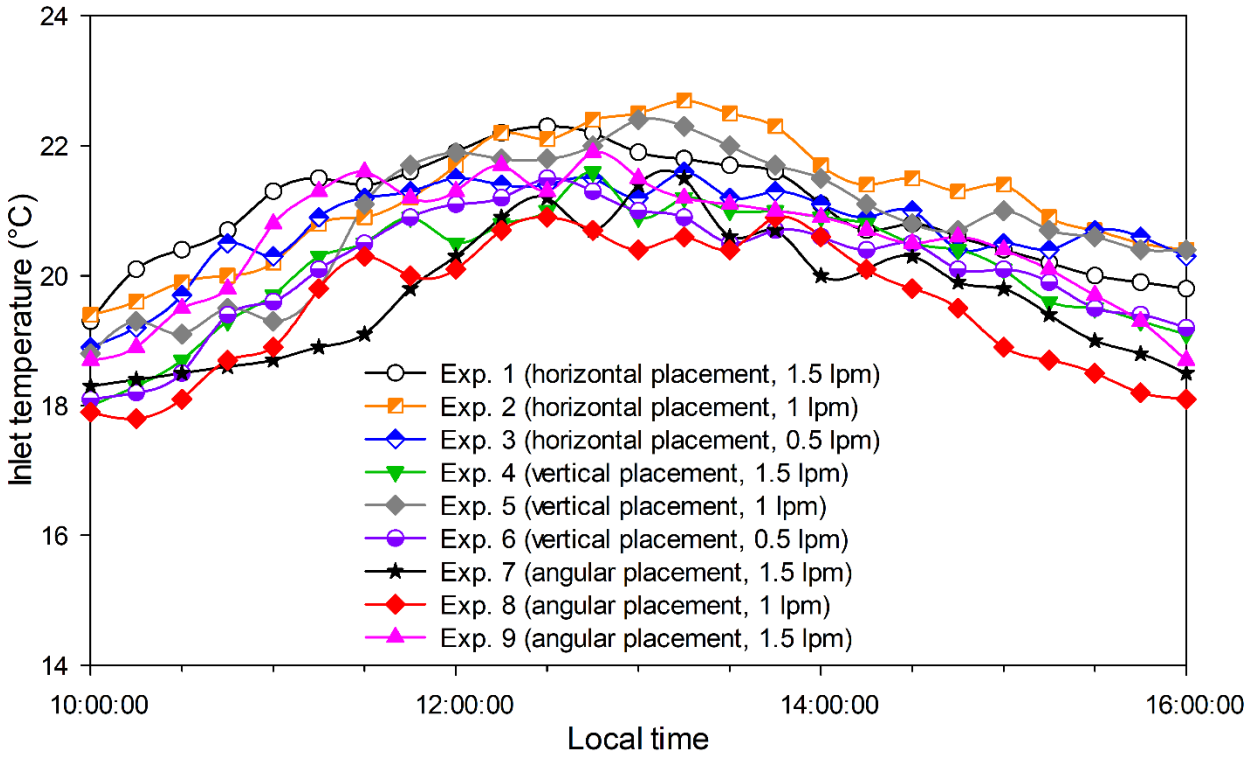

Fig. 13. Time-dependent change in inlet water temperatures

Fig. 14 represents a time-dependent change in outlet water temperatures and gained heat at different orientations of a helically-coiled solar collector. In the horizontal orientation of the solar collector, average outlet temperatures at 1.5, 1.0 and 0.5 lpm were recorded as 21.83°C, 22.29°C, and 22.31°C, respectively. Average outlet temperature values in the vertical orientation of helically-coiled solar collector were obtained as 20.92°C, 21.77°C and 21.40°C, at 1.5, 1.0, and 0.5 lpm flow rates, respectively. Also, for angular orientation of the helically-coiled solar collector mean outlet temperature values at 1.5, 1.0, and 0.5 lpm volumetric water flow rates were achieved as 20.90°C, 20.99°C, and 22.67°C, respectively. In the performance tests done at the lowest water volumetric flow rate, outlet temperature values at angular orientations (Exp. 7) were high in comparison with other placements. In addition, the average value of the temperature difference between the water outlet and inlet of the solar collector in horizontal, vertical

and angular orientations were achieved between the ranges of 0.82-1.55°C, 0.76-1.28°C, and 1.16-2.12°C, respectively. Moreover, mean gained useful energy values at horizontal, vertical, and angular orientations were obtained in the ranges of 64.96-102.45 W, 53.56-95.41W, and 88.89-145.6 W, respectively.

Fig. 15 illustrates the time-dependent change in thermal efficiency values for different orientations of helically-coiled solar water collectors. Average thermal efficiency values for Exp. 1, Exp. 2, and Exp. 3 were gained as 48.23%, 41.94%, and 29.48%, respectively. Also, mean efficiency values for Exp. 4, 5, and 6 were achieved as 47.03%, 38.21%, and 27.17%, respectively. In addition, average thermal efficiency values for angular orientations (Exp. 7, Exp. 8, and Exp. 9) were gained as 52.71%, 44.06%, and 32.50%, respectively. Moreover, a comparison between the thermal efficiencies of solar collectors at different orientations and the same volumetric flow rate is presented in Fig. 16. This figure clearly shows the higher thermal efficiency of the angular orientation of the helically coiled solar collector.

GCRIS

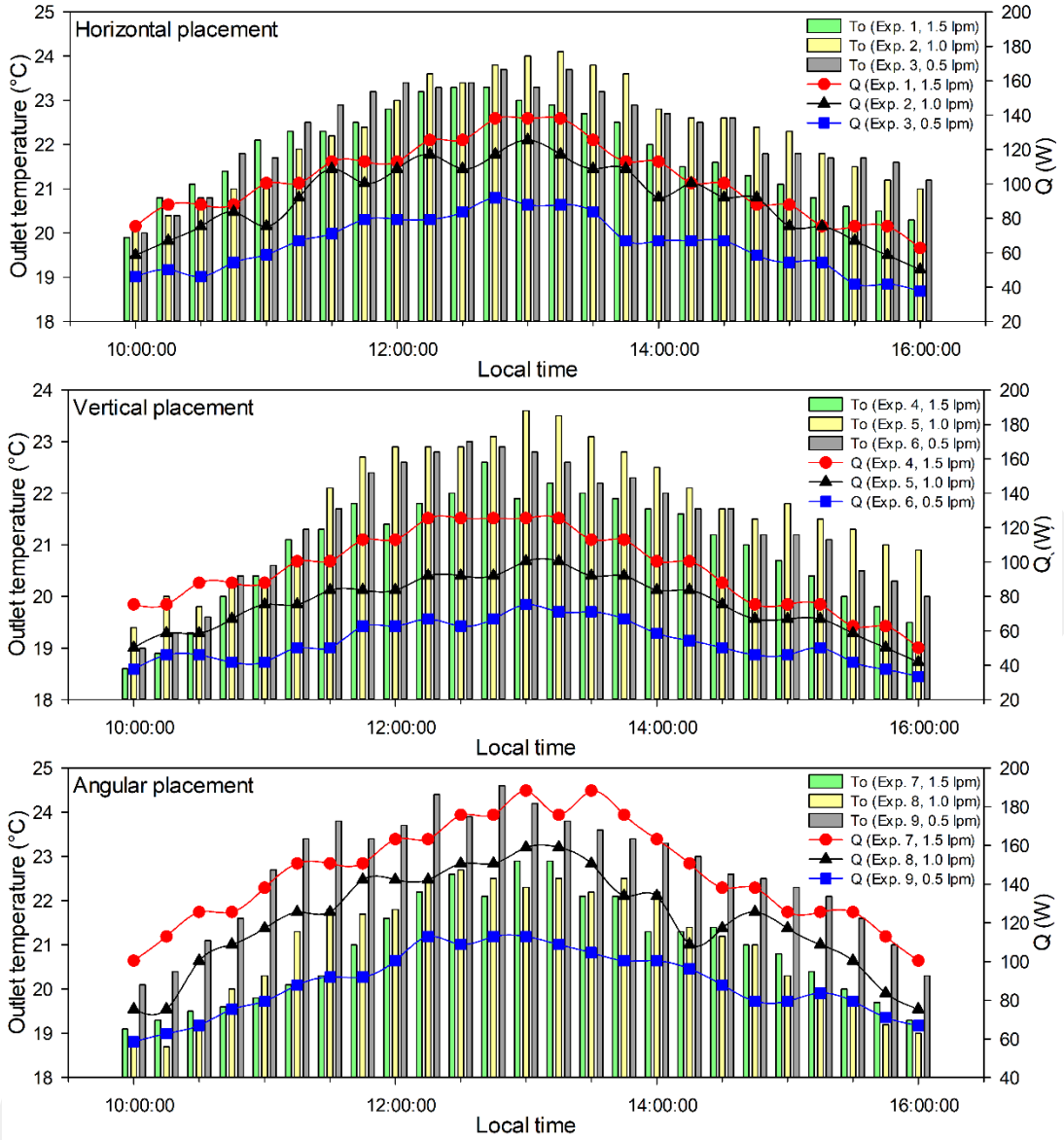

Fig. 14. Time-dependent change in outlet water temperatures and gained heat

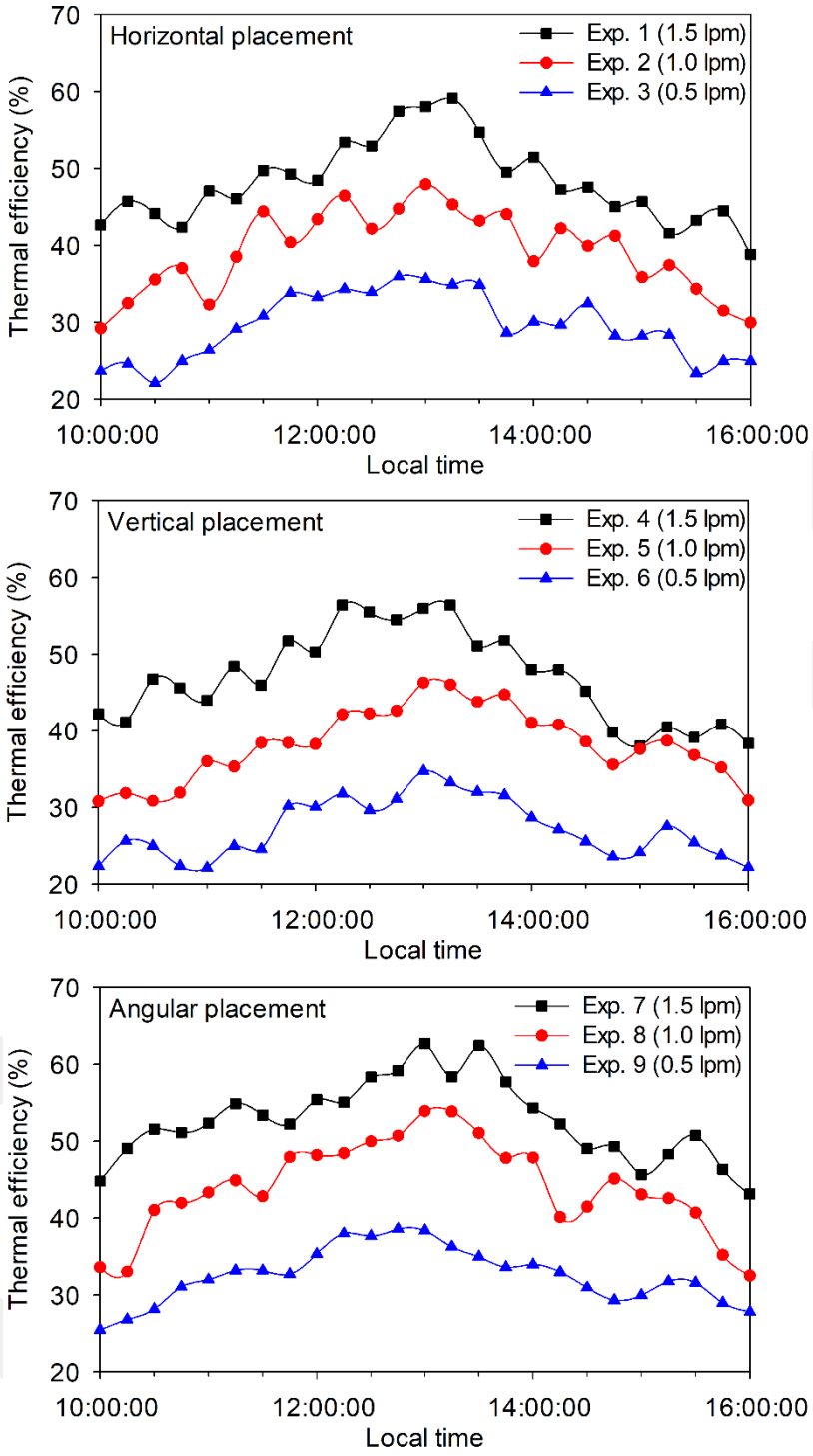

Fig. 15. Time-dependent variation in thermal efficiency values of solar water collector

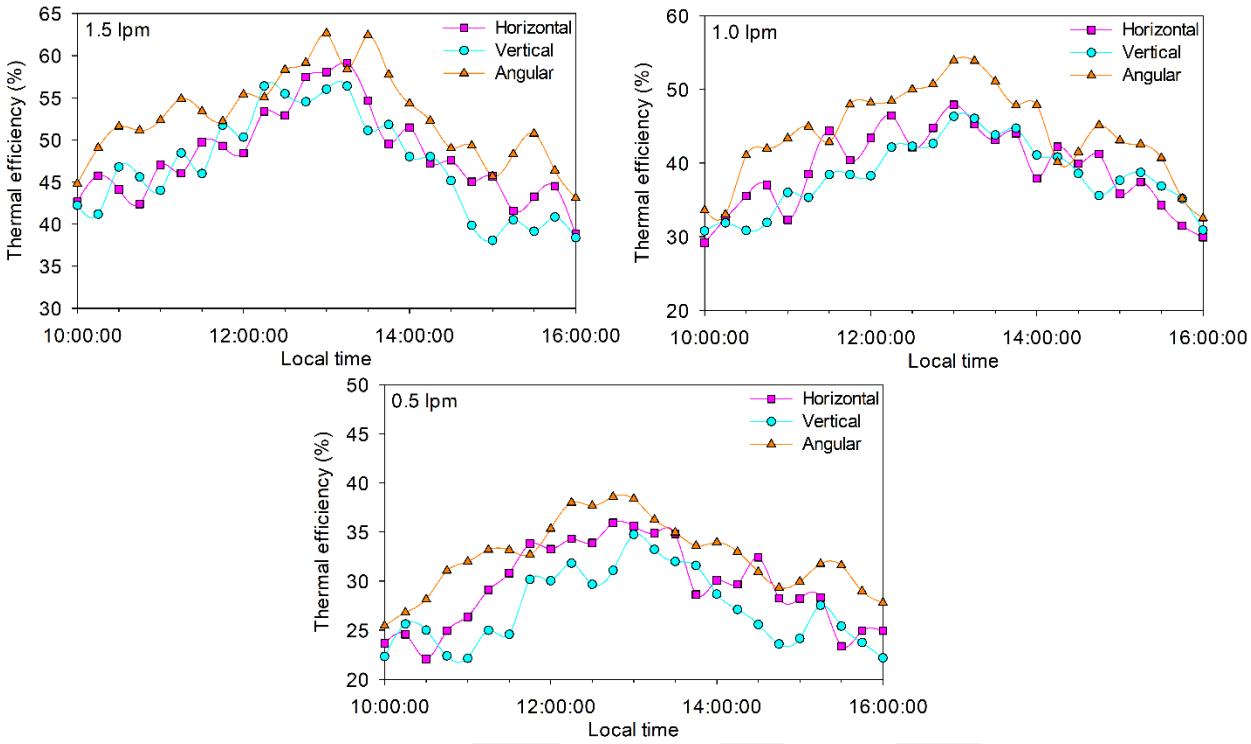

Fig. 16. Comparison between thermal efficiency values of solar collector at different orientations

Fig. 17 presents the time-dependent variation in exergy efficiency values for various orientations of helically-coiled solar water collector. Generally, it can be stated that exergy efficiency values and thermal efficiency values showed similar trends. However, variations in environmental conditions like ambient temperature led to some differences. Mean exergy efficiency values for horizontal, vertical, and angular orientation of helically-coiled solar collector were achieved in the ranges of 0.40-0.90%, 0.38-0.86%, and 0.43-1.01%, respectively. In a study, Vengadesan and Senthil (2022) developed a flat plate-type water collector equipped with a bifunctional turbulator and obtained an exergy efficiency of up to 3.30%. In another academic work, Vengadesan et al. (2022)

investigated a hybrid flat plate solar collector and achieved average exergy efficiency between 1.35-2.31%.

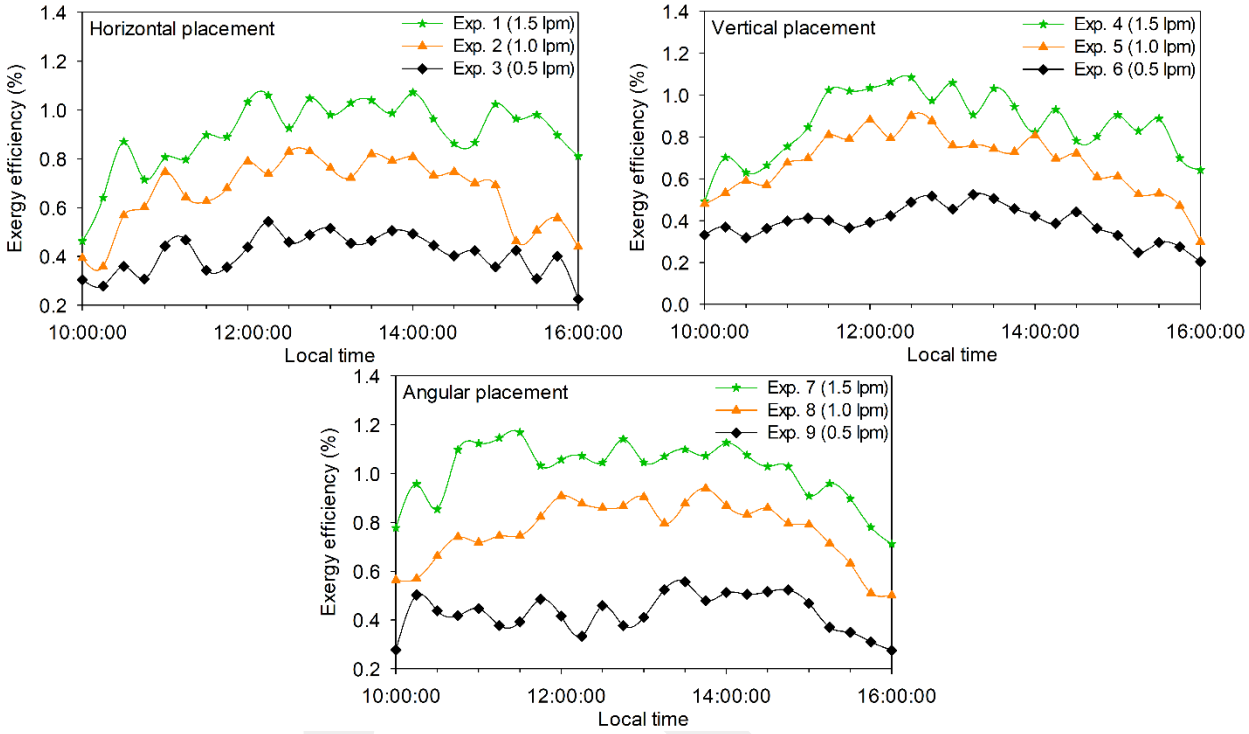

Fig. 17. Time-dependent variation in exergy efficiency values

Fig. 18 represents experimentally obtained average SI values for different orientations of helically-coiled solar collector at different orientations. SI values for horizontal, vertical and angular orientations were obtained in the ranges of 1.0041-1.0091, 1.0039-1.0087 and 1.0043-1.0102, respectively. Similar SI values were attained in a research that analyzed a solar water collector (Caliskan, 2017).

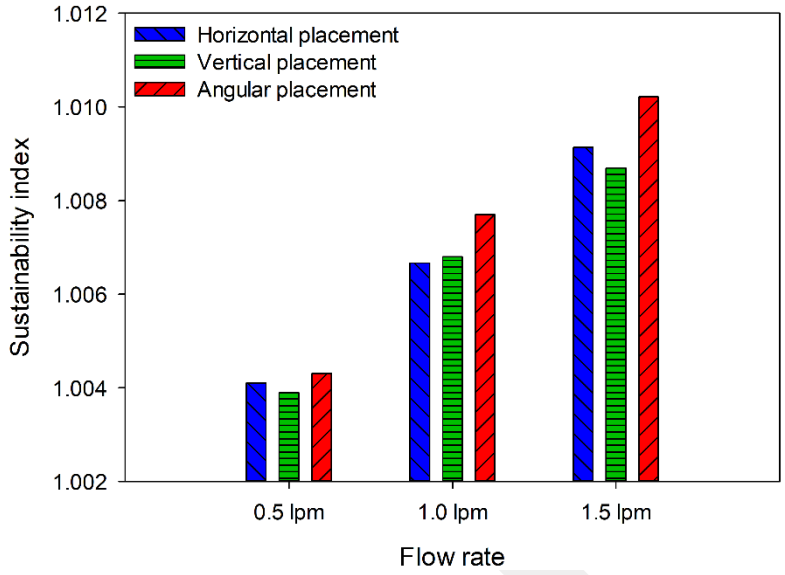

Fig. 18. Experimentally obtained average SI values

Fig. 19 represents a comparison of experimentally and numerically obtained gained thermal energy values at various water flow rates. According to the obtained findings, deviation between experimental and numerical results were obtained in the ranges of 6.5-14%.

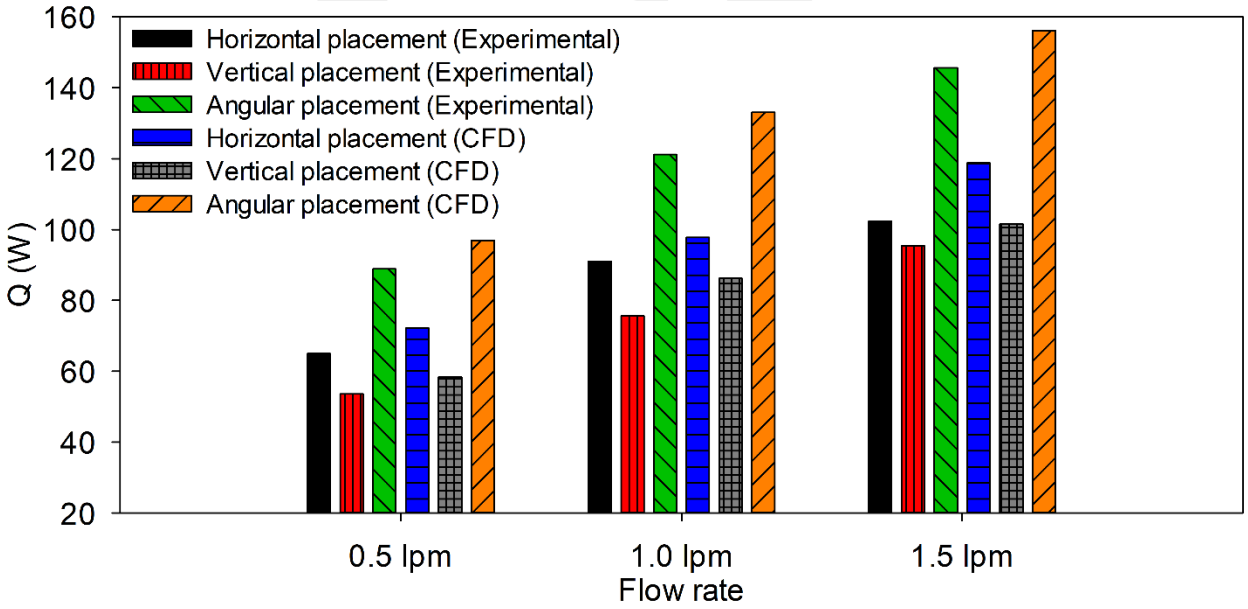

Fig. 19. Comparison of experimentally and numerically obtained gained thermal energy values

Table 3 illustrates a comparison between the gained thermal efficiency values in this study with available works. Analyzing the thermal efficiency of related studies indicated the good performance of the developed helically-coiled solar water collector in this study. In some studies, different approaches like using turbulators and changing working fluid with nanofluids have been applied in order to enhance the thermal efficiency of the solar collectors.

The general outcomes of this experimental and numerical research exhibited the successfulness of the designed helically-coiled solar collector. Using the helically coiled design in water collectors is a new topic in literature. According to the performed literature review, there are so few similar works that have tested the performance of collectors just in a horizontal position. The present study is adding valuable data about this design in three different assembly positions (horizontal, angular, and vertical). Besides that, the simulation model provides supporting data for comparing the performance of different configurations of the proposed collector.

517 **Table 3.** Comparison of gained thermal efficiency values with related works available in
518 the open literature

Ref.	Collector type	Test location	Flow rate	Thermal efficiency
Moravej et al. (2020)	Flat plate water collector	Aghajari, Iran	0.005833-0.046667 L/s	~50-62% for water, ~52-83% for nanofluid
Pathak et al. (2019b)	Dual-purpose storage equipped solar water and air collector	India	0.025-0.04167 kg/s	~35-82%
Hao et al. (2018)	Flat plate dual-function solar collector	Shandong, China	-	32.5-50.8%
Somwanshi and Sarkar (2020)	Flat plate dual-function solar collector	Raipur, Chhattisgarh, India	0.005, 0.007, 0.010, 0.015, 0.020 kg/s	~ 46-84%
Goudarzi et al. (2014)	Helically-coiled solar water collector	Yasouj, Iran	0.0083, 0.0167 and 0.033 kg/s	~10-70%
Goudarzi et al. (2015)	Helically-coiled solar water collector	Iran	0.0083 kg/s	~0.05-75%
This work	Helically-coiled solar water collector	Ankara, Turkey	0.5-1.5 lpm	27.17-52.71%

519

520 **5. Conclusion**

521 In this study, a solar water collector with a helically-coiled absorber has been designed,
522 fabricated, and experimentally tested. Also, the CFD method has been used in order to
523 specify the flow and thermal behavior of the developed helically-coiled collector. In this

524 regard, the designed helically-coiled collector has been investigated at different
525 orientation angles numerically and experimentally. The major outcomes of the current
526 study can be given as:

527 • Mean gained useful energy values at horizontal, vertical and angular orientations
528 were obtained in the ranges of 64.96-102.45 W, 53.56-95.41W and 88.89-145.6
529 W, respectively.
530 • Thermal efficiency values of horizontal, vertical, and angular helically-coiled
531 collector were obtained in the ranges of 29.48-48.23%, 27.17-47.03%, and 32.50-
532 52.71%, respectively. Adjusting the tilt angle of the collector improved the thermal
533 efficiency between the ranges of 12.07-19.62%. Moreover, the maximum
534 increment in thermal efficiency by increasing the flow rate and adjusting the tilt
535 angle of the collector was attained as 93.98%.
536 • Sustainability index values for horizontal, vertical, and angular helically-coiled
537 collectors were achieved between the ranges of 1.0041-1.0091, 1.0039-1.0087,
538 and 1.0043-1.0102, respectively.

539 The experimental and numerical outcomes of this study exhibited the applicability of a
540 helically-coiled tube as an absorber of a solar water collector. Also, it was seen that the
541 orientation of a helically-coiled collector has a significant effect on thermal performance.
542 In the next studies, different modifications could be done in order to gain more thermal
543 performance. In addition, the developed collector within the scope of this work can be
544 integrated to a closed-loop system and heat transfer fluids that have a high thermal
545 conductivity in comparison to water such as nanofluids can be tested to improve the

efficiency of the current design. Moreover, concentrators can be integrated to the system to improve the receiving solar irradiance on the absorber surface (helically coiled tube).

References

Abo-Elfadl, S., Hassan, H., El-Dosoky, M.F., (2020). Study of the performance of double pass solar air heater of a new designed absorber: An experimental work. Solar Energy 198, 479-489.

Abo-Elfadl, S., Yousef, M. S., El-Dosoky, M. F., Hassan, H. (2021). Energy, exergy, and economic analysis of tubular solar air heater with porous material: an experimental study. Applied Thermal Engineering, 196, 117294.

Afshari, F., Karagoz, S., Comakli, O., Ghasemi Zavaragh, H. (2019). Thermodynamic analysis of a system converted from heat pump to refrigeration device. Heat and Mass Transfer, 55(2), 281-291.

Afshari, F., Sözen, A., Khanlari, A., Tuncer, A.D., Şirin, C. (2020). Effect of turbulator modifications on the thermal performance of cost-effective alternative solar air heater. Renewable Energy 158, 297-310.

Afshari, F., Tuncer, A. D., Sözen, A., Çiftçi, E., Khanlari, A. (2021). Experimental and numerical analysis of a compact indirect solar dehumidification system. Solar Energy, 226, 72-84.

Akbar, A., Najafi, G., Gorjian, S., Kasaeian, A., Mazlan, M. (2021). Performance enhancement of a hybrid photovoltaic-thermal-thermoelectric (PVT-TE) module using nanofluid-based cooling: Indoor experimental tests and multi-

568 objective optimization, Sustainable Energy Technologies and Assessments,
569 46, 101276.
570 Almeshaal, M., Arunprasad, V., Palaniappan, M., Kolsi, L. (2020). Experimental study of
571 a solar water heater fitted with spacer at the leading edge of Left-Right screw
572 tapes. Case Studies in Thermal Engineering, 22, 100777.
573 Amini, A., Özdemir, T., Ekici, Ö., Başlamışlı, S. Ç., Köksal, M. (2021). A thermal model
574 for Li-ion batteries operating under dynamic conditions. Applied Thermal
575 Engineering, 185, 116338.
576 Ansys, ANSYS Fluent Theory Guide, ANSYS Inc, Canonsburg, 2017.
577 Awasthi, K., Khan, M. K. (2019). Performance evaluation of coiled tube receiver cavity for
578 a concentrating collector. Renewable Energy, 138, 666-674.
579 Aytaç, İ. (2022a). Experimental investigation on heat transfer performance of
580 Fe_2O_3/Water AND Fe_3O_4/Water nanofluids in a plate heat exchanger. Heat
581 Transfer Research, 53(15), 69-93.
582 Aytaç, İ. (2022b). Determination of the thermal behavior of water-based Fe_3O_4 nanofluid
583 using thermophysical property models. Heat Transfer Research, 53(18), 57-
584 75.
585 Caliskan, H. (2017). Energy, exergy, environmental, enviroeconomic,
586 exergoenvironmental (EXEN) and exergoenviroeconomic (EXENEC)
587 analyses of solar collectors. Renewable and Sustainable Energy Reviews,
588 69, 488-492.
589 Cengel, Y., Cimbala, J. (2013). Fluid Mechanics Fundamentals and Applications, 3rd
590 Edition, McGraw-Hill Education, New York, NY.

591 Çengel, Y., Ghajar, A., (2020). Heat and Mass Transfer-Fundamentals and Applications,
592 6th Edition, McGraw-Hill Education, New York, NY.
593 Chakraborty, O., Roy, S., Das, B., Gupta, R. (2021). Effects of helical absorber tube on
594 the energy and exergy analysis of parabolic solar trough collector–A
595 computational analysis. Sustainable Energy Technologies and Assessments,
596 44, 101083.
597 Eker, M., Yarımpabuç, D., Çelebi, K. (2021). Thermal stress analysis of functionally
598 graded solid and hollow thick-walled structures with heat generation.
599 Engineering Computations, 38 (1), 371-391.
600 El-Said, E. M., Abou Al-Sood, M. M., Elsharkawy, E. A., Abdelaziz, G. B. (2022). Tubular
601 solar air heater using finned semi-cylindrical absorber plate with swirl flow:
602 Experimental investigation. Solar Energy, 236, 879-897.
603 Fattahi, A., Karimi, N. (2022). Numerical simulation of the effects of superhydrophobic
604 coating in an oval cross-sectional solar collector with a wavy absorber filled
605 with water-based Al2O3-ZnO-Fe3O4 ternary hybrid nanofluid. Sustainable
606 Energy Technologies and Assessments, 50, 101881.
607 Ghodbane, M., Bellos, E., Said, Z., Boumeddane, B., Hussein, A. K., Kolsi, L. (2021).
608 Evaluating energy efficiency and economic effect of heat transfer in copper
609 tube for small solar linear Fresnel reflector. Journal of Thermal Analysis and
610 Calorimetry, 143(6), 4197-4215.
611 Gholipour, S., Afrand, M., Kalbasi, R. (2020). Improving the efficiency of vacuum tube
612 collectors using new absorbent tubes arrangement: introducing helical coil
613 and spiral tube adsorbent tubes. Renewable Energy, 151, 772-781.

614 Gholipour, S., Afrand, M., Kalbasi, R. (2021). Introducing two scenarios to enhance the
615 vacuum U-tube solar collector efficiency by considering economic criterion.
616 Journal of the Taiwan Institute of Chemical Engineers, 124, 228-237.
617 Gorjian, S., Hosseingholilou, B., Jathar, L.D., Samadi, H., Samanta, S., Sagade, A.A.,
618 Kant, K. Sathyamurthy, R. (2021). Recent Advancements in Technical
619 Design and Thermal Performance Enhancement of Solar Greenhouse
620 Dryers. Sustainability 13, 7025.
621 Goudarzi, K., Shojaeizadeh, E., Nejati, F. (2014). An experimental investigation on the
622 simultaneous effect of CuO–H_2O nanofluid and receiver helical pipe on the
623 thermal efficiency of a cylindrical solar collector. Applied Thermal
624 Engineering, 73(1), 1236-1243.
625 Goudarzi, K., Nejati, F., Shojaeizadeh, E., Yousef-Abad, S. A. (2015). Experimental study
626 on the effect of pH variation of nanofluids on the thermal efficiency of a solar
627 collector with helical tube. Experimental Thermal and Fluid Science, 60, 20-
628 27.
629 Hao, W., Lu, Y., Lai, Y., Yu, H., Lyu, M. (2018). Research on operation strategy and
630 performance prediction of flat plate solar collector with dual-function for drying
631 agricultural products. Renewable Energy, 127, 685-696.
632 Hassan, H., Abo-Elfadl, S., El-Dosoky, M.F., (2020). An experimental investigation of the
633 performance of new design of solar air heater (tubular). Renewable Energy,
634 151, 1055-1066.
635 Kansara, R., Pathak, M., Patel, V. K. (2021). Performance assessment of flat-plate solar
636 collector with internal fins and porous media through an integrated approach

637 of CFD and experimentation. International Journal of Thermal Sciences, 165,
638 106932.
639 Khanlari, A., Sözen, A., Tuncer, A. D., Afshari, F., Gürbüz, E. Y., Bilge, Y. C. (2021).
640 Numerical and experimental analysis of longitudinal tubular solar air heaters
641 made from plastic and metal waste materials. Heat Transfer Research, 52
642 (10), 19-45.
643 Khanlari, A., Tuncer, A. D., Sözen, A., Aytaç, İ., Çiftçi, E., Variyenli, H. İ. (2022). Energy
644 and exergy analysis of a vertical solar air heater with nano-enhanced
645 absorber coating and perforated baffles. Renewable Energy, 187, 586-602.
646 Kotas, T.J., 1995. The Exergy Method of Thermal Plant Analysis. Krieger Publish
647 Company, UK, Malabar, FL.
648 Lewis, R. W., Malan, A. G., 2005. Continuum thermodynamic modeling of drying capillary
649 particulate materials via an edge-based algorithm. Computer methods in
650 applied mechanics and engineering, 194, 2043-2057.
651 https://doi.org/10.1615/ICHMT.2004.IntThermSciSemin.180.
652 Li, G. (2015). Energy and exergy performance assessments for latent heat thermal
653 energy storage systems. Renewable and sustainable energy reviews, 51,
654 926-954.
655 Li, G. (2016). Sensible heat thermal storage energy and exergy performance evaluations.
656 Renewable and Sustainable Energy Reviews, 53, 897-923.
657 Li, G., Zheng, X. (2016). Thermal energy storage system integration forms for a
658 sustainable future. Renewable and Sustainable Energy Reviews, 62, 736-
659 757.

660 Nithiarasu, P., Lewis, R. W., Seetharamu, K. N. (2016). Fundamentals of the finite
661 element method for heat and mass transfer. John Wiley & Sons.
662 Malan, A. G., Lewis, R. W., 2003. Continuum thermodynamic modeling of drying capillary
663 particulate materials using an unstructured finite volume algorithm. In
664 Computational Fluid and Solid Mechanics 2003, 1434-1437.
665 Moravej, M., Bozorg, M. V., Guan, Y., Li, L. K., Doranehgard, M. H., Hong, K., Xiong, Q.
666 (2020). Enhancing the efficiency of a symmetric flat-plate solar collector via
667 the use of rutile TiO_2-water nanofluids. Sustainable Energy Technologies and
668 Assessments, 40, 100783.
669 Pathak, P. K., Chandra, P., Raj, G. (2019). Comparative analysis of modified and
670 convectional dual purpose solar collector: Energy and exergy analysis.
671 Energy Sources, Part A: Recovery, Utilization, and Environmental Effects, 1-
672 17.
673 Pathak, P. K., Chandra, P., Raj, G. (2019). Comparative analysis of single-and dual-
674 purpose corrugated plate solar collector by force convection. Heat Transfer—
675 Asian Research, 48(6), 2387-2401.
676 Petela, R., 2003. Exergy of undiluted thermal radiation. Sol. Energy 74, 469-488.
677 Ramanathan, S., Thansekhar, M. R., Kanna, P. R., Gunnasegaran, P. (2020). A new
678 method of acquiring perquisites of recirculation and vortex flow in sudden
679 expansion solar water collector using vortex generator to augment heat
680 transfer. International Journal of Thermal Sciences, 153, 106346.

Rani, P., Tripathy, P. P. (2022). Experimental investigation on heat transfer performance of solar collector with baffles and semicircular loops fins under varied air mass flow rates. International Journal of Thermal Sciences, 178, 107597.

Raut, D., Lanjewar, S., Kalamkar, V. R. (2022). Effect of geometrical and operational parameters on paraffin's melting performance in helical coiled latent heat storage for solar application: A numerical study. International Journal of Thermal Sciences, 176, 107509.

Saedodin, S., Zaboli, M., Ajarostaghi, S. S. M. (2021). Hydrothermal analysis of heat transfer and thermal performance characteristics in a parabolic trough solar collector with Turbulence-Inducing elements. Sustainable Energy Technologies and Assessments, 46, 101266.

Sarper, B., Saglam, M., Aydin, O. (2018). Experimental and numerical investigation of natural convection in a discretely heated vertical channel: Effect of the blockage ratio of the heat sources. International Journal of Heat and Mass Transfer, 126, 894-910.

Sarper, B., Saglam, M., Aydin, O., Avci, M. (2018). Natural convection in a parallel-plate vertical channel with discrete heating by two flush-mounted heaters: effect of the clearance between the heaters. Heat and Mass Transfer, 54(4), 1069-1083.

Selimefendigil, F., Şirin, C. (2022). Energy and exergy analysis of a hybrid photovoltaic/thermal-air collector modified with nano-enhanced latent heat thermal energy storage unit. Journal of Energy Storage, 45, 103467.

703 Selimefendigil, F., Şirin, C., Öztop, H. F. (2022). Experimental performance analysis of a
704 solar desalination system modified with natural dolomite powder integrated
705 latent heat thermal storage unit. Sustainability, 14, 2650.
706 Singla, M., Hans, V. S., Singh, S. (2022). CFD analysis of rib roughened solar evacuated
707 tube collector for air heating. Renewable Energy, 183, 78-89.
708 Sheikholeslami, M., Ebrahimpour, Z. (2022). Thermal improvement of linear Fresnel solar
709 system utilizing Al_2O_3-water nanofluid and multi-way twisted tape.
710 International Journal of Thermal Sciences, 176, 107505.
711 Sheikholeslami, M., Farshad, S. A. (2021). Investigation of solar collector system with
712 turbulator considering hybrid nanoparticles. Renewable Energy, 171, 1128-
713 1158.
714 Sheikholeslami, M., Farshad, S. A., Shafee, A., Babazadeh, H. (2021). Performance of
715 solar collector with turbulator involving nanomaterial turbulent regime.
716 Renewable Energy, 163, 1222-1237.
717 Sheikholeslami, M., Jafaryar, M. (2023). Thermal assessment of solar concentrated
718 system with utilizing CNT nanoparticles and complicated helical turbulator.
719 International Journal of Thermal Sciences, 184, 108015.
720 Sheikholeslami, M., Jafaryar, M., Said, Z., Alsabery, A. I., Babazadeh, H., Shafee, A.
721 (2021). Modification for helical turbulator to augment heat transfer behavior
722 of nanomaterial via numerical approach. Applied Thermal Engineering, 182,
723 115935.

Sheikholeslami, M., Said, Z., Jafaryar, M. (2022). Hydrothermal analysis for a parabolic solar unit with wavy absorber pipe and nanofluid. Renewable Energy, 188, 922-932.

Shojaeizadeh, E., Veysi, F., Habibi, H., Goodarzi, K., Habibi, M. (2021). Thermal efficiency investigation of a ferrofluid-based cylindrical solar collector with a helical pipe receiver under the effect of magnetic field. Renewable Energy, 176, 198-213.

Somwanshi, A., Sarkar, N. (2020). Thermal performance of a dual-purpose collector-cum-storage type air-water heater. Applied Thermal Engineering, 171, 115094.

Sözen, A., Sirin, C., Khanlari, A., Tuncer, A.D., Gürbüz, E.Y., (2020). Thermal performance enhancement of tube-type alternative indirect solar dryer with iron mesh modification. Solar Energy 207, 1269-1281.

Swanepoel, J. K., le Roux, W. G., Lexmond, A. S., Meyer, J. P. (2021). Helically coiled solar cavity receiver for micro-scale direct steam generation. Applied Thermal Engineering, 185, 116427.

Tiwari, A., Dubey, S., Sandhu, G.S., Sodha, M.S., Anwar, S.I., 2009. Exergy analysis of integrated photovoltaic thermal solar water heater under constant flow rate and constant collection temperature modes. Appl Energy 86 (12), 2592–2597.

Vengadesan, E., Bharathwaj, D., Kumar, B.S., Senthil, R., (2022). Experimental study on heat storage integrated flat plate solar collector for combined water and air heating in buildings. Applied Thermal Engineering, 216, 119105.

Vengadesan, E., Senthil, R. (2022). Experimental study on the thermal performance of a flat plate solar water collector with a bifunctional flow insert. Sustainable Energy Technologies and Assessments, 50, 101829.

Wong, K.F.V., 2000. Thermodynamics for Engineers. University of Miami/CRC Press LLC, Taylor & Francis, USA.

Xiong, Q., Altnji, S., Tayebi, T., Izadi, M., Hajjar, A., Sundén, B., Li, L. K. (2021). A comprehensive review on the application of hybrid nanofluids in solar energy collectors. Sustainable Energy Technologies and Assessments, 47, 101341.

Xiong, Q., Tayebi, T., Izadi, M., Siddiqui, A. A., Ambreen, T., Li, L. K. (2021). Numerical analysis of porous flat plate solar collector under thermal radiation and hybrid nanoparticles using two-phase model. Sustainable Energy Technologies and Assessments, 47, 101404.

Yazdanpanahi, J., Sarhaddi, F., Adeli, M. M. (2015). Experimental investigation of exergy efficiency of a solar photovoltaic thermal (PVT) water collector based on exergy losses. Solar Energy, 118, 197-208.

Yıldırım, A., Eker, M., Yarımpabuç, D., Celebi, K. (2021). Thermal wave propagation in a functionally graded annular fin with fixed base. Waves in Random and Complex Media, https://doi.org/10.1080/17455030.2021.1925175.

Zou, Y., Li, X., Yang, L., Zhang, B., Wu, X. (2023). Efficient direct absorption solar collector based on hollow TiN nanoparticles. International Journal of Thermal Sciences, 185, 108099.